


Article

Desorption of REEs from Halloysite and Illite: A Link to the Exploitation of Ion-Adsorption RE Ore Based on Clay Species

Sen Qiu ^{1,2}, Huashan Yan ^{1,2,*} , Bengen Hong ³, Qibang Long ², Jie Xiao ², Fujian Li ^{1,4}, Lichao Tong ³, Xiaowen Zhou ^{1,2} and Tingsheng Qiu ^{1,2,*}

¹ Collaborative Innovation Center for Development and Utilization of Rare Metal Resources Co-Sponsored by Ministry of Education and Jiangxi Province, Jiangxi University of Science and Technology, Ganzhou 341000, China

² College of Resource and Environmental Engineering, Jiangxi University of Science and Technology, Ganzhou 341000, China

³ Longyan Rare Earth Development Co., Ltd., Longyan 361000, China

⁴ Beijing Key Laboratory of Ionic Liquids Clean Process, State Key Laboratory of Multiphase Complex Systems, CAS Key Laboratory of Green Process and Engineering, Institute of Process Engineering, Chinese Academy of Sciences, Beijing 100045, China

* Correspondence: jxustyhs@163.com (H.Y.); 9019810001@jxust.edu.cn (T.Q.); Tel.: +86-152-9776-3712 (H.Y.); +86-138-0358-7811 (T.Q.)

Abstract: The adsorption/desorption characteristics for light and heavy rare earth elements (REEs) on halloysite and illite (which are beneficial for the utilization of ion-adsorption RE ore) were systematically investigated and compared. Additionally, halloysite and illite were fully characterized by XRD, SEM, microscope, zeta potential, nitrogen adsorption–desorption isotherms and buffer pH to build the relationship between adsorption/desorption mechanisms and the minerals' properties. The results of experiments show that the adsorption rate of halloysite is higher than illite, although they are both very fast and follow the pseudo-second-order kinetic model. The adsorption capacity of halloysite and illite increases with an increase in adsorption pH and remains constant when pH is higher than 4. Due to the narrow interlamellar spacing of halloysite and the fact that it is a nanotube, RE ions are adsorbed only through electrostatic attraction, whereas the adsorption and desorption pH have a significant effect on the recovery of RE ions from illite, because of the diverse adsorption mechanism. The results illustrated that the structure and surface properties of clays are also the key factors that affect RE ions leaching.

Keywords: rare earth; clays; adsorption; desorption; electrostatic attraction



Citation: Qiu, S.; Yan, H.; Hong, B.; Long, Q.; Xiao, J.; Li, F.; Tong, L.; Zhou, X.; Qiu, T. Desorption of REEs from Halloysite and Illite: A Link to the Exploitation of Ion-Adsorption RE Ore Based on Clay Species. *Minerals* **2022**, *12*, 1003. <https://doi.org/10.3390/min12081003>

Academic Editors: Manuel Pozo Rodríguez, Francisco Franco and Michael G. Stamatakis

Received: 2 July 2022

Accepted: 7 August 2022

Published: 8 August 2022

Publisher's Note: MDPI stays neutral with regard to jurisdictional claims in published maps and institutional affiliations.



Copyright: © 2022 by the authors. Licensee MDPI, Basel, Switzerland. This article is an open access article distributed under the terms and conditions of the Creative Commons Attribution (CC BY) license (<https://creativecommons.org/licenses/by/4.0/>).

1. Introduction

It is well-known that rare earth elements (REEs) are widely used in advanced materials and high-technology fields, including permanent magnets, luminescence, catalysts and alloys [1–4], especially for heavy REEs (Y, Tb, Dy, Ho, Er, Tm, Yb and Lu), which mainly come from ion-adsorption rare earth (RE) ore. Ion-adsorption RE ore is a unique mineral that is formed by the following processes [5]: the RE original rocks (granitic and volcanic) are weathered under humid and warm climate conditions; meanwhile, the RE ions are released from weathered original rocks and migrated with rainwater and groundwater; subsequently, the released RE ions are adsorbed onto electronegative clay mineral surfaces such as halloysite and illite [6–9]. Hence, the ion-adsorption RE ore is exploited by ion-exchange with inorganic salt solutions, such as NH_4^+ and Mg^{2+} solutions [10]. A geography study revealed that the content of clay in ion-adsorption RE ore decreases in the order of halloysite > illite > kaolinite > montmorillonite [11]. However, the influence of clay mineral species is not considered during the leaching process, although there are obvious distinctions for the desorption characteristics of RE ions from different clays.

Halloysite is a hollow nanotube with a length of 600–1000 nm, and an inner and outer radius of 30 nm and 100 nm, respectively [12]. It is typically a 1:1 silicate mineral ($\text{Al}_2\text{O}_3 \cdot 2\text{SiO}_2 \cdot 4\text{H}_2\text{O}$), where tetrahedral SiO_4 (Si-O layer) is in the exterior face, and the inner face has an octahedral AlO_6 [13]. As for illite, which is 2:1 laminar silicate mineral, the top and bottom layers are tetrahedral SiO_4 and mixed with an octahedral AlO_6 in the middle [14]. There are several similar properties for halloysite and illite, such as the fact that surface hydroxyls can be protonated and deprotonated [15], which has an effect on the adsorption mechanism of RE ions on clay surfaces. Their surfaces are electronegative due to isomorphous substitution; however, the points of zero charge (PZC), buffer pH and specific surface area (SSA) of halloysite and illite would be different, which is crucial information for the adsorption of RE ions.

To better understand the mineralization process of ion-adsorption RE ore, the investigation of RE ion adsorption on raw clay minerals is an effective method [16–18]. Gao et al. [19] studied the influence of pH, Na^+ and K^+ ions on the adsorption of RE ions onto kaolinite and halloysite; they indicated that kaolinite mainly adsorbed heavy REEs while halloysite adsorbed lighter REEs, if there is K^+ in solution. In addition, Yang et al. [20] investigated the adsorption of complete RE ions series on kaolinite and halloysite under different pH levels and ionic strengths, and concluded that both kaolinite and halloysite preferentially adsorbed heavy REEs at high ionic strength and high pH, while without apparent fractionation at low ionic strengths. However, this work only focused on the adsorption process, with no attention to the desorption process. Hence, Alshameri et al. [21] systematically studied and compared the adsorption/desorption for La^{3+} and Yb^{3+} of kaolinite, montmorillonite, muscovite and illite, and found that kaolinite has highest desorption efficiencies for La^{3+} (89%) and Yb^{3+} (85%) in the order of kaolinite > illite > montmorillonite > muscovite, while the presence of iron oxide in muscovite led to the low desorption efficiencies of RE ions. However, this study concentrated on single-RE ions adsorbed on clays, with little attention to the adsorption/desorption of mixed-RE ions, which would have competition effects on each other. Additionally, the adsorption/desorption characteristics of light/heavy RE ions on different clays would be different. Hence, halloysite and illite, as the dominant hosts for RE ions in ion-adsorption RE ore [11], deserve more attention.

The objective of this work is to investigate the adsorption and desorption characteristics of light and heavy RE ions from halloysite and illite, clarify the differences, and build the relationship between leaching technology of ion-adsorption RE ore and clay species, in order to form classified leaching technology based on the clay species. The adsorption capacity, adsorption kinetics, desorption rate, desorption agent concentration and effects of pH of Nd^{3+} , Eu^{3+} and Lu^{3+} from halloysite and illite were studied. The X-ray diffraction (XRD), zeta potential, N_2 adsorption–desorption isotherms and buffer pH of halloysite and illite were determined and compared to reveal the adsorption mechanism. This study obtained a new insight into the classificatory leaching technology of ion-adsorption RE ore based on clay species.

2. Materials and Methods

2.1. Materials

Halloysite and illite were sourced from Yunnan and Zhejiang provinces, China, respectively. All the chemicals used, such as neodymium chloride, europium chloride, lutetium chloride, ammonium sulfate, hydrochloric acid, sulfuric acid and sodium hydroxide, are of analytical grade.

2.2. Characterization of Halloysite and Illite

Powder X-ray diffraction (XRD) was determined between 5° to 70° (2θ) with a step size of 0.02 using a Bruker Smart Apex II with $\text{Cu-K}\alpha$ ($\lambda = 0.154$ nm) radiation operating at 40 kV and 40 mA; the illite sample was prepared by side charging to avoid preferred orientation. Scanning electron microscopy (SEM) analysis was performed by FEI- MLA650F.

The clays were ultrasonically for 5 min before being deposited and then were coated with a thin shell of gold by sputter deposition; images were taken in secondary electron mode with an accelerating voltage of 20.0 kV and working distance of 13.6 mm. The image of polarizing microscope was photographed by a Leica DM2700 P.

Zeta potentials were determined by a Malvern Zetasizer Nano ZS 90 instrument. A total of 5 mg of halloysite/illite was added into 50 mL of deionized water to obtain suspensions (0.1 mg/mL), and ultrasonically for 10 min; subsequently, the supernate was used for tests. Both 0.1 mol/L HCl and 0.1 mol/L NaOH solutions were used to adjust the pH of suspensions in a range of 2.5 to 6.

N₂ adsorption–desorption isotherms were measured at 77 K for five hours with 0.5 g clays on a BSD 3H-2000PS2 instrument. The specific surface area (SBET) was calculated using the multiple-point Brunauer–Emmett–Teller (BET) method.

In order to investigate the buffer performance of halloysite and illite, 2 g of halloysite/illite was mixed with 16 mL of pH = 3.0, 4.1, 5.1, 6.1, 7.2, 7.9, 8.9, 10.0, 11.0 aqueous phase, respectively, and then shaken for 120 min in conical flasks in a mechanical shaker. After that, aqueous phase was separated by centrifugation at 6000 rpm for 2 min and filtered by a microfiltration membrane. The residual H⁺ ion was determined by a pH meter.

2.3. Batch Adsorption Experiments

Chloride neodymium, europium and lutetium were mixed in a solution with the concentration of 0.46 mmol/L for each REE. All batch adsorption experiments were carried out using conical flasks in a mechanical shaker with halloysite (or illite)/liquid ratio of 1:25. The mixtures were shaken with a constant speed of 200 rpm at a temperature of 25 °C for a given time. Subsequently, the adsorbents were separated by centrifuge and rinsed with deionized water several times. After that, the adsorbents were dissolved with nitric acid, hydrochloric acid, sulfuric acid and perchloric acid, and then the concentrations of Nd³⁺, Eu³⁺ and Lu³⁺ were determined by inductively coupled plasma optical emission spectrometry (ICP-OES). The equilibrium adsorption capacities (q_e) of adsorbents were calculated by using the following equation:

$$q_e = \frac{m}{M} \quad (1)$$

where q_e is adsorption capacity (mg/g), m and M are the mass of adsorbed REEs and adsorbents, respectively.

2.3.1. Adsorption Kinetics Experiments

The optimum time required for the Nd³⁺, Eu³⁺ and Lu³⁺ was determined as a function of contact time in the range of 1 min–240 min at a fixed pH of 5 and 25 °C. Clay samples of 0.6 g were mixed with 15 mL of Nd³⁺, Eu³⁺ and Lu³⁺ solution at every individual time point.

2.3.2. Influence of Initial pH on Adsorption

In order to evaluate the effect of initial pH on adsorption, the adsorbents were mixed with RE ion solution in a pH range of 2 to 6, and the equilibrium solution's pH was determined.

2.4. Batch Desorption Experiments

The adsorption pH not only affects adsorption capacity, but also influences the adsorption stability of RE ions. Hence, the adsorbents that adsorbed RE ions in a pH range of 2 to 5.8 were desorbed by a pH = 4 0.11 mol/L (NH₄)₂SO₄ (solid/liquid = 1:50) solu-

tion for 240 min. Desorption efficiencies for halloysite and illite were calculated by the following equation:

$$\text{Recovery (\%)} = \frac{CV}{m q_e} \times 100 \quad (2)$$

where C is the REE concentration in solution after desorption, V is the volume of desorption solution, m and q_e are the mass and adsorption capacity of adsorbents, respectively.

The effect of desorption pH, contact time and $(\text{NH}_4)_2\text{SO}_4$ concentration on desorption of RE ions from halloysite and illite were investigated with a solid/liquid rate of 1:50. The adsorbents that were used in the desorption process were prepared in the same way as the adsorption test at pH = 5 and contact 240 min. In order to obtain the optimal desorption pH of RE ions from halloysite and illite, the recovery of Nd^{3+} , Eu^{3+} , and Lu^{3+} was determined as a function of desorption pH in the range of 2.5 to 6, and the equilibrium pH was determined. The influence of contact time was studied in the range of 1 min to 240 min at the optimal desorption pH. The optimal $(\text{NH}_4)_2\text{SO}_4$ concentration was investigated in the range of 0 to 0.19 mol/L.

3. Results and Discussion

3.1. Characterization of Halloysite and Illite

3.1.1. XRD and SEM Analysis

XRD, SEM and polarizing a microscope were used to characterize halloysite and illite. Figure 1 shows XRD patterns of characteristic diffraction peaks (2θ) of halloysite-7 Å and illite- $2M_1$ at 11.96° , 19.87° , 8.86° and 17.65° ; the corresponding interplanar distances are 7.42, 4.46, 10.07 and 5.04, which illustrates that they are composed almost entirely of raw clay mineral [19,22]. XRD shows that the largest interplanar distances of illite (002) is higher than halloysite (001), which is beneficial for the crossing of RE ions. In order to verify the purity of clays once more, SEM and a polarizing microscope were used and the results are shown in Figure 2; it can be found that halloysite is a tubulose, which is the conspicuous distinction with kaolinite. Additionally, the polarizing microscope results (Figure 2d) of illite show that there are almost no lumps under $2\text{ }\mu\text{m}$, implying that there is no muscovite.

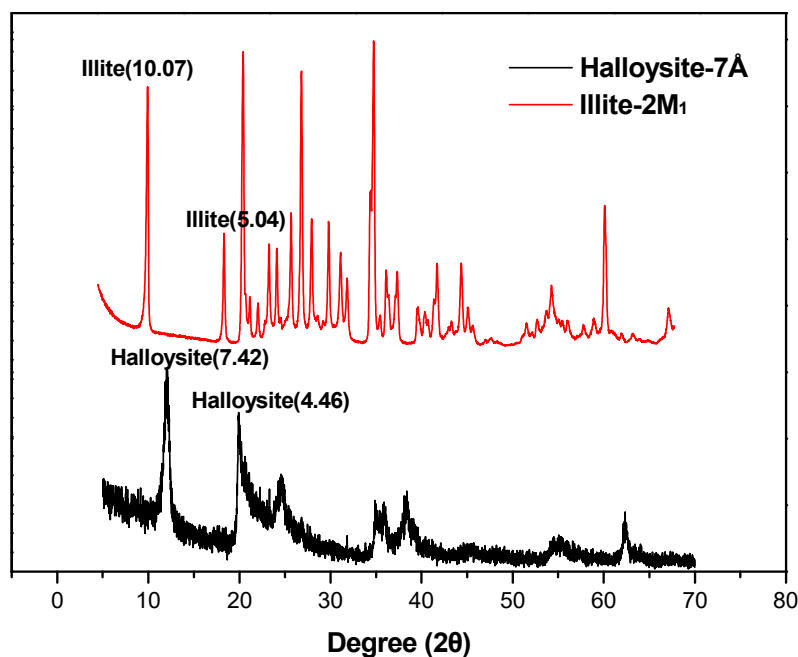


Figure 1. XRD patterns for halloysite and illite.

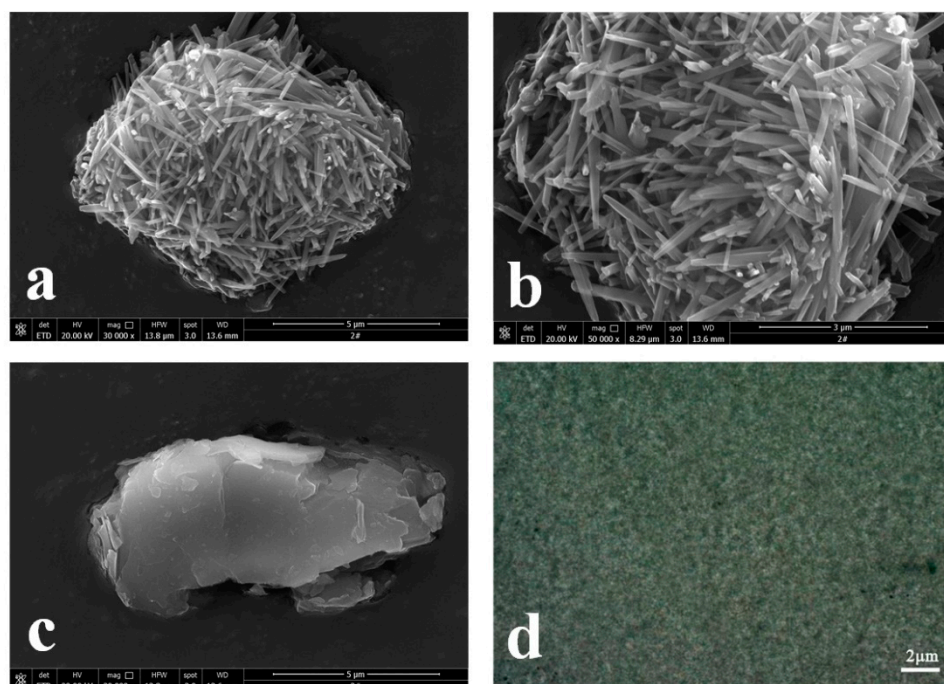


Figure 2. SEM (a–c) and microscope (d) images for halloysite (a,b) and illite (c,d).

3.1.2. Zeta Potential

Previous works revealed that most RE ions are adsorbed on clays by electrostatic force [23,24]; hence, the surface charge of halloysite and illite is crucial for the adsorption of Nd^{3+} , Eu^{3+} and Lu^{3+} . Figure 3 shows the zeta potential of halloysite and illite as a function of pH between 2.5 and 6. It shows that the zeta potentials of halloysite and illite decrease with an increase in pH, suggesting that higher pH contributed to negative charge on the surfaces of adsorbents. Positively charged ions prefer to adsorb on negatively charged surfaces, which provides the driving force for electrostatic interaction with RE ions [25]. Hence, the adsorption capacity of RE ions on halloysite and illite would increase with the increase in solution pH. On the other hand, zeta potentials of halloysite and illite are similar in the test pH range, and change to positive at pH 2.5, implying that the adsorption capacity of halloysite is comparable to that of illite, and low pH goes against adsorbing RE ions.

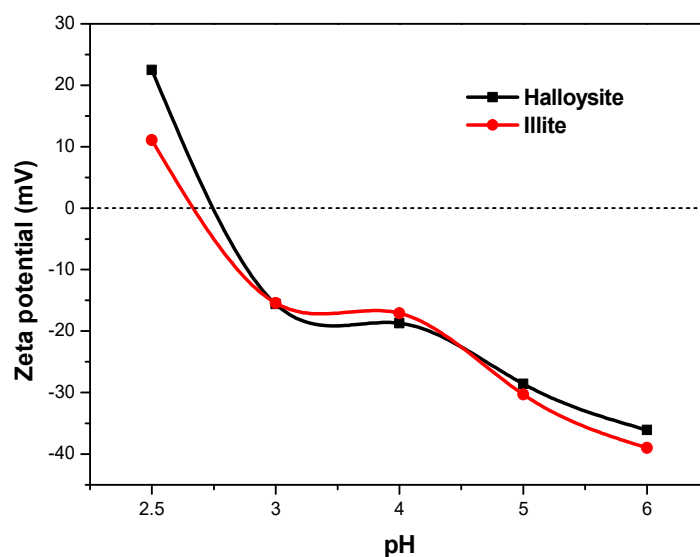


Figure 3. Zeta potential of halloysite and illite as a function of pH.

3.1.3. Specific Surface Area

N₂ adsorption–desorption isotherms were applied to measure the specific surface area of halloysite and illite, and the results are shown in Figure 4. The adsorption–desorption isotherms of halloysite and illite show a characteristic hysteresis loop, which is associated with capillary condensation in the mesopores. The SBET and pore volume of halloysite are 24.87 m²/g and 0.1854 cm³/g (Table 1), which is much higher than illite (6.78 m²/g, 0.0423 cm³/g) because halloysite is hollow nanotube, while illite is a tightly stacked lamellar, as shown in SEM images (Figure 2). Generally, high SBET is beneficial for the adsorption capacity.

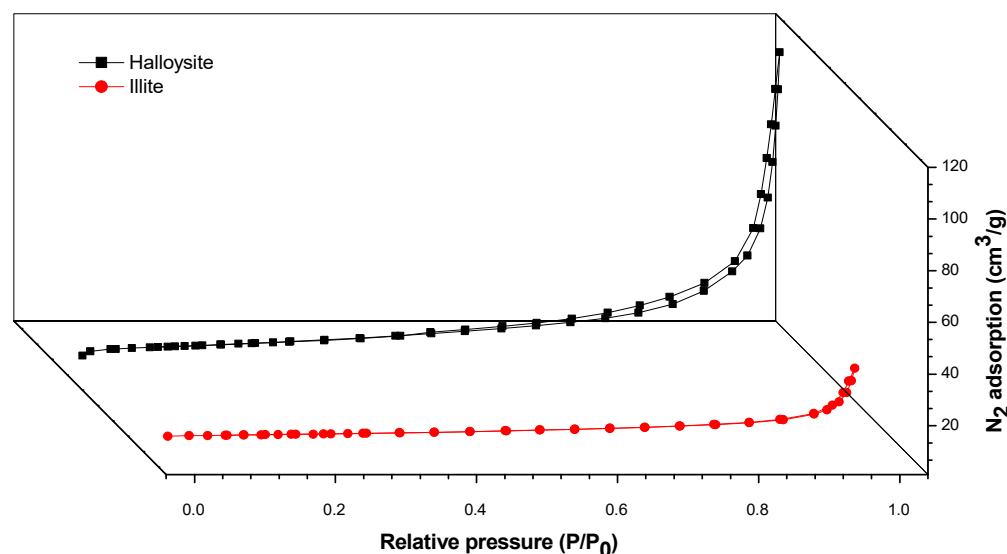


Figure 4. The adsorption–desorption isotherms of halloysite and illite.

Table 1. Specific surface area, pore volume and pore diameter (nm) of halloysite and illite.

| Clays | SBET (m ² /g) | Pore Volume (cm ³ /g) | Pore Diameter (nm) |
|-------------------|--------------------------|----------------------------------|--------------------|
| Halloysite | 24.87 | 0.1854 | 29.81 |
| Illite | 6.78 | 0.0423 | 24.94 |

3.1.4. Buffer Performance

The surface hydroxyl of halloysite and illite can protonate and deprotonate depending on the solution pH, which is crucial for the adsorption of RE ions. Buffer capacity of halloysite and illite at different initial solution pH values are observed (Figure 5). It is shown that equilibrium pH levels of halloysite and illite stabilize at 5.3 and 6.7, respectively, when initial pH is in the range of 4 to 10. On the other hand, it is overflowing when initial pH levels are 3 and 11. Because the protonation/deprotonation sites of halloysite and illite were limited, plenty of H⁺/OH[−] were dissociated in the solution while initial acidity/basicity is high. These results reveal that halloysite and illite would protonate or deprotonate while solution pH levels are higher or lower than 5.3 and 6.7, respectively. The buffer pH levels indicate that halloysite and illite can almost be protonated in raw water, which goes against them adsorbing RE ions by surface complex.

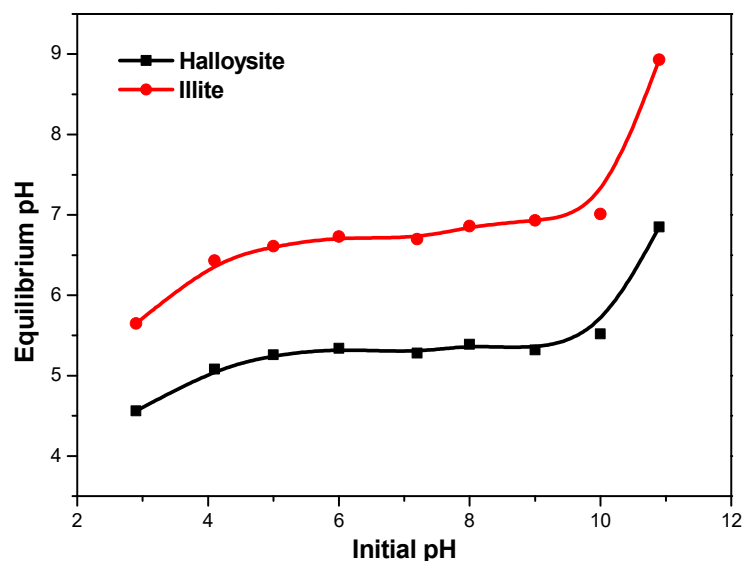


Figure 5. Buffer performance of halloysite and illite at different initial solution pH values.

3.2. Adsorption Characteristics of Nd^{3+} , Eu^{3+} and Lu^{3+} onto Halloysite and Illite

3.2.1. Adsorption Kinetics

Figure 6 shows the q_e of Nd^{3+} , Eu^{3+} and Lu^{3+} on halloysite and illite as a function of contact time. It can be found that the q_e of Nd^{3+} , Eu^{3+} and Lu^{3+} on halloysite and illite increases quickly with an increase in contact time and reaches equilibrium in 60 min; beyond this value, there is no noticeable increase in the adsorption. Most RE ions are adsorbed within 5 min ($\sim 95\%$), indicating that the adsorption of RE ions on clays is quite rapid. This might be ascribed to the utilization of readily available adsorption sites of the clays, resulting in a fast diffusion and rapid equilibrium attainment [21]. The short equilibrium time indicates an excellent affinity of clays for RE ions [26]. The q_e of Lu^{3+} is slightly higher than Nd^{3+} and Eu^{3+} due to a larger atomic weight of Lu, suggesting there is no apparent fractionation for light and heavy REEs on halloysite and illite. Despite the fact that the SBET of halloysite is larger than illite, the q_e of halloysite is smaller than illite, which may be due to the narrow interlamellar spacing of halloysite (7 Å), which goes against the interaction between RE ions and active surface sites.

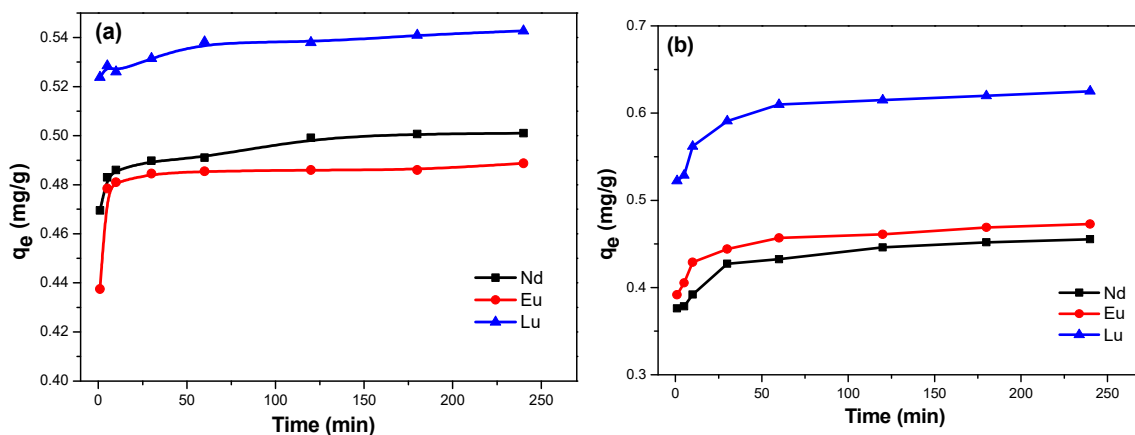


Figure 6. Effect of contact time on Nd^{3+} , Eu^{3+} and Lu^{3+} adsorption onto halloysite (a) and illite (b).

In order to investigate the adsorption kinetics of Nd^{3+} , Eu^{3+} and Lu^{3+} on halloysite and illite, the pseudo-first-order [27] and pseudo-second-order [28] models were applied to simulate the kinetics behavior, and corresponding equations are shown as follows:

The pseudo-first-order model:

$$\ln(q_e - q_t) = \ln q_e - k_1 t \quad (3)$$

The pseudo-second-order model:

$$\frac{t}{q_t} = \frac{1}{q_e} t + \frac{1}{k_2 q_e^2} \quad (4)$$

where q_e and q_t are the adsorption capacity at equilibrium and time t , respectively, and k_1 and k_2 are rate constants of pseudo-first-order and pseudo-second-order models, respectively.

The adsorption kinetics of Nd^{3+} , Eu^{3+} and Lu^{3+} on halloysite and illite are shown in Figure 7 and the corresponding kinetics parameters of pseudo-first-order and pseudo-second-order models are listed in Table 2. The correlation coefficient values (R^2) are 0.999 for the pseudo-second-order model, which is higher than that of the pseudo-first-order model, and the calculated q_e values of the pseudo-second-order model fit well with experimental values. The results imply that the kinetics adsorptions of Nd^{3+} , Eu^{3+} and Lu^{3+} on halloysite and illite can be described by the pseudo-second-order model very well, which means that both concentration of RE ions and the number of active sites on clays can influence the adsorption rate [29]. Meanwhile, the larger k_2 values indicate that the adsorption rate of RE ions on halloysite is higher than on illite, which is attributed to outer-layer adsorptions that interact by electrostatic force.

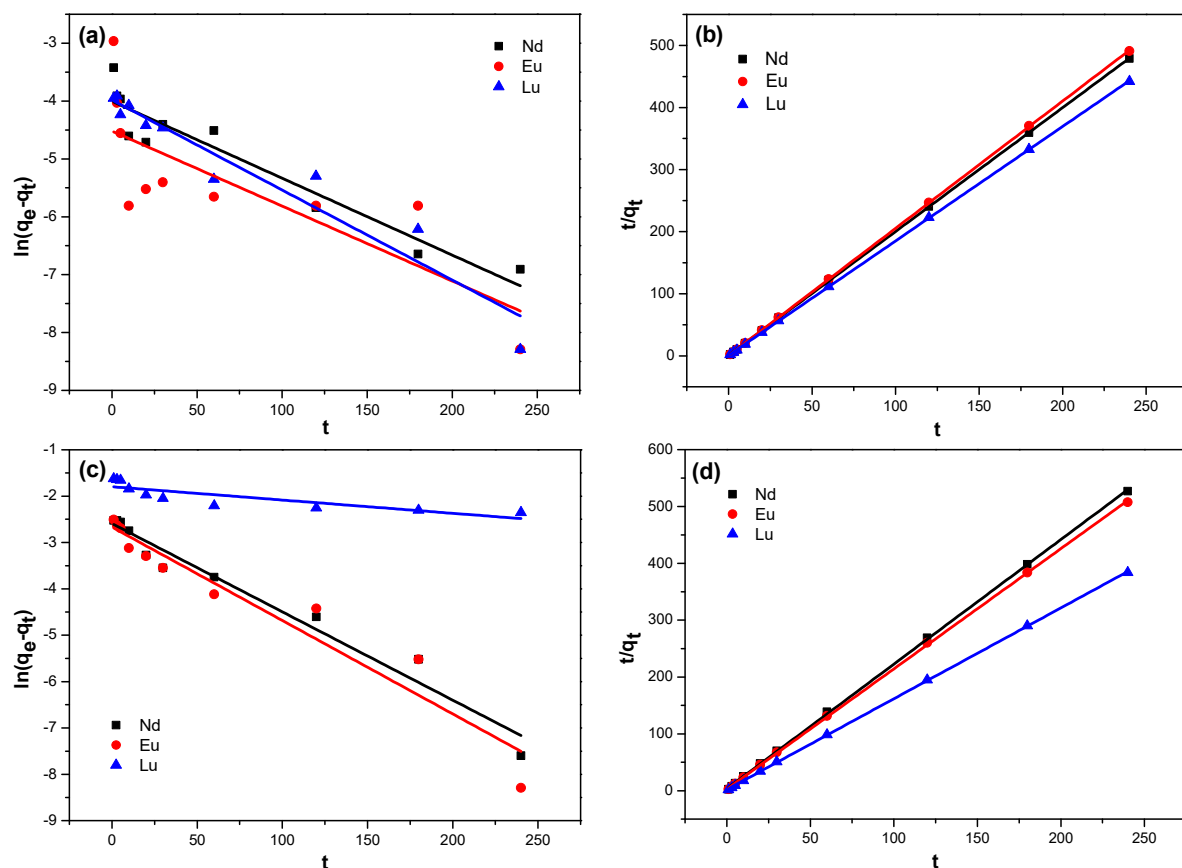


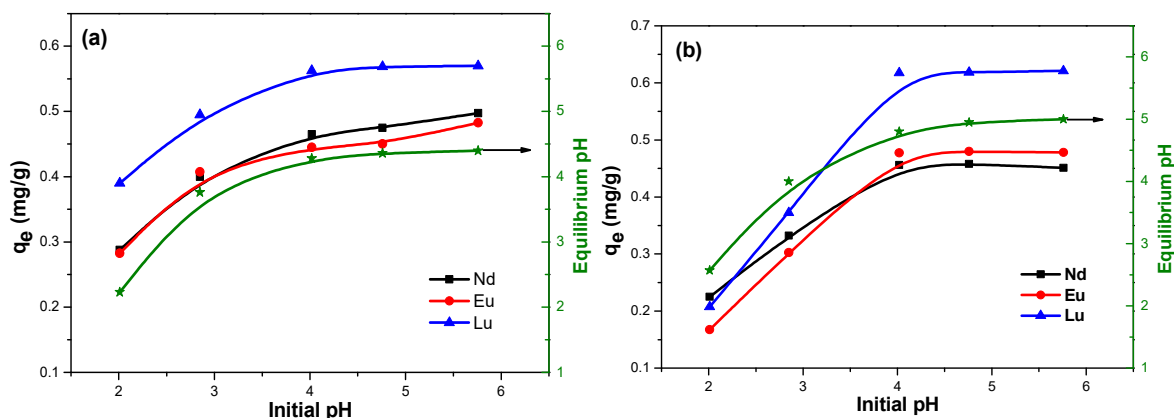
Figure 7. Pseudo-first order, pseudo-second order for Nd^{3+} , Eu^{3+} and Lu^{3+} on halloysite (a,b) and illite (c,d).

Table 2. Kinetics parameters for the adsorption of Nd^{3+} , Eu^{3+} and Lu^{3+} on halloysite and illite.

| Species | Pseudo-First Order | | | Pseudo-Second Order | | |
|------------|--------------------|-----------------------------|-------|---------------------|------------------|-------|
| | q_e (mg/g) | k_1 (min^{-1}) | R^2 | q_e (mg/g) | k_2 (mg/g/min) | R^2 |
| Halloysite | | | | | | |
| Nd | 0.018 | 0.0133 | 0.903 | 0.501 | 5.19 | 0.999 |
| Eu | 0.011 | 0.0129 | 0.545 | 0.488 | 11.37 | 0.999 |
| Lu | 0.018 | 0.0156 | 0.919 | 0.542 | 5.38 | 0.999 |
| Illite | | | | | | |
| Nd | 0.075 | 0.019 | 0.963 | 0.456 | 1.42 | 0.999 |
| Eu | 0.069 | 0.02 | 0.922 | 0.473 | 1.66 | 0.999 |
| Lu | 0.081 | 0.017 | 0.942 | 0.625 | 1.40 | 0.999 |

3.2.2. Effect of pH on Adsorption Capacity

One of the vital factors which affects the adsorption behavior of RE ions is the pH of solution. The q_e of Nd^{3+} , Eu^{3+} and Lu^{3+} on halloysite and illite as a function of solution pH is shown in Figure 8. It can be seen that the q_e of all RE ions on halloysite and illite increase with an increase in initial pH and nearly reaches equilibrium at a pH level of 4. The lower q_e at low initial pH is caused by two reasons: one is of ZPC, which is the main driving force for RE ions adsorbed on clay surfaces, and low pH values contribute to the small absolute value of ZPC (Figure 3), which goes against RE ions adsorbing on clay surfaces; on the other hand, the presence of more H^+ in an overly acidic solution leads to greater competitive adsorption between H^+ and RE ions [30]. Previous analysis showed that the ZPC of halloysite and illite is similar, while the SBET of halloysite is much higher than illite, whereas the adsorption capacity of halloysite is lower than illite, which may be due to the narrow interlamellar spacing of halloysite where RE ions cannot pass through.

**Figure 8.** Effect of initial pH on Nd^{3+} , Eu^{3+} and Lu^{3+} adsorption on halloysite (a) and illite (b).

The equilibrium pH levels after Nd^{3+} , Eu^{3+} and Lu^{3+} adsorb on halloysite and illite were determined (Figure 8). It shows that the equilibrium pH levels diverge from initial pH due to the buffer performance of halloysite and illite. Moreover, the equilibrium pH levels reach a platform when initial pH is higher than 4, which is same as the tendency of q_e . The results indicate that q_e is influenced by equilibrium pH rather than initial pH. However, the equilibrium pH levels of halloysite and illite are lower than their buffer pH (Figure 5), implying that the adsorption of RE ions is beneficial for H^+ fleeing from clay surfaces.

3.3. Desorption Characteristics of Nd^{3+} , Eu^{3+} and Lu^{3+} from Halloysite and Illite

3.3.1. Influence of Adsorption pH on RE Ion Desorption

Adsorption pH plays a vital role in the q_e of RE ions on halloysite and illite; on the other hand, it also influences the adsorption mechanism [31,32]. Figure 9 shows the

recovery of Nd^{3+} , Eu^{3+} and Lu^{3+} from halloysite and illite as a function of adsorption pH. The recovery of Nd^{3+} , Eu^{3+} and Lu^{3+} from halloysite decreases slightly with the increase in adsorption pH (100.1% at pH 2, 97.5% at pH 6), which proves that pH has negligible influence on the adsorption mechanism of RE ions on halloysite within the tested pH range. The high recovery (>96%) at all tested pH ranges reveals that RE ions are adsorbed on halloysite surfaces mainly by electrostatic attraction. However, the recovery of Nd^{3+} , Eu^{3+} and Lu^{3+} from illite decreases with an increase in adsorption pH. This may be attributed to the different adsorption mechanisms under various pH conditions. Similar to kaolinite [33], RE ions adsorbed on illite by weakly electrostatic attraction, while illite surfaces are deprotonated at low acidic solution, and coordination bonds are formed between RE ions and illite surfaces [34].

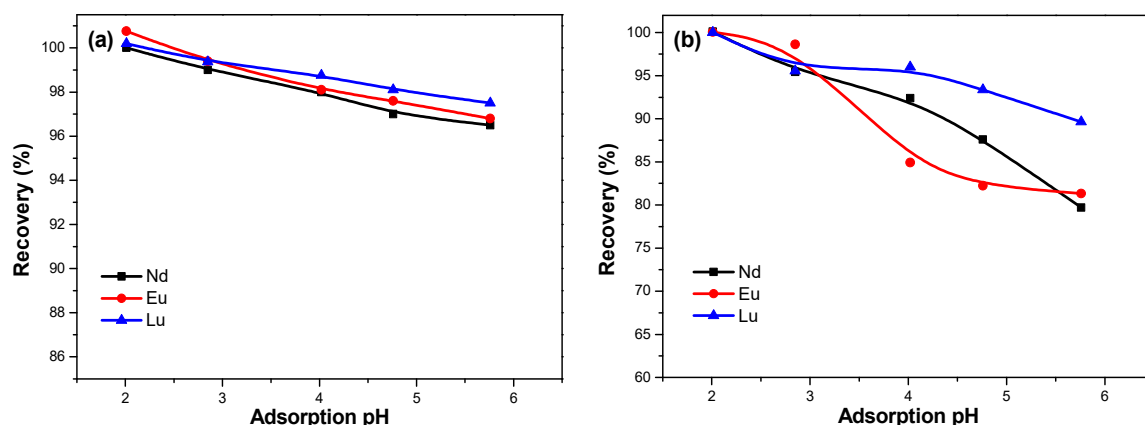


Figure 9. Effect of adsorption pH on the recovery of Nd^{3+} , Eu^{3+} and Lu^{3+} from halloysite (a) and illite (b). (pH = 4.2, contact time = 240 min, $(\text{NH}_4)_2\text{SO}_4$ concentration = 0.11 mol/L).

3.3.2. Influence of pH on RE Ion Desorption

The recovery of Nd^{3+} , Eu^{3+} and Lu^{3+} from halloysite and illite as a function of desorption pH is shown in Figure 10. Similar to the effect of adsorption pH, the recovery of Nd^{3+} , Eu^{3+} and Lu^{3+} from halloysite decreases slightly with an increase in initial pH, while it decreases more drastically for illite. As mentioned earlier, RE ions are adsorbed on halloysite surfaces mainly by electrostatic attraction, which can be easily desorbed by ion exchange; hence, the recovery almost maintains a constant as a function of initial pH. As for illite, the desorption pH has a significant effect on the recovery of RE ions. RE ions that are adsorbed through coordination bonds are hard to be desorbed by ion exchange, but they can change to outer-layer adsorption by electrostatic attraction at low-pH solutions, which are easy to be desorbed. Hence, the recovery of RE ions increases with a decrease in pH, whereas the RE ions that recovered under the high-pH condition are adsorbed by electrostatic attraction, and the residual might be adsorbed through coordination bonds, which only desorbed with low-pH solutions. The equilibrium pH is different to initial pH due to the buffer performance of halloysite and illite; hence, solid/liquid rates need to be considered when determining desorption pH. Hence, the optimal desorption pH levels in the following desorption experiments for halloysite and illite are 4 and 3, respectively.

3.3.3. Influence of Lixiviate Concentration on RE Ion Desorption

Figure 11 shows the influence of $(\text{NH}_4)_2\text{SO}_4$ concentration on the recovery of Nd^{3+} , Eu^{3+} and Lu^{3+} from halloysite and illite. The recovery increases quickly with an increase in $(\text{NH}_4)_2\text{SO}_4$ concentration. The recovery of RE ions from halloysite is only ~3% without $(\text{NH}_4)_2\text{SO}_4$, while it is ~50% from illite, because the pH of the leaching agent for illite is 3, which is lower than halloysite, indicating that a part of RE ions can be desorbed by H^+ . The recovery of Nd^{3+} and Lu^{3+} from halloysite is 88% and 81% when $(\text{NH}_4)_2\text{SO}_4$ concentration is 0.011 mol/L, and then slightly increases with an increase in $(\text{NH}_4)_2\text{SO}_4$

concentration until 0.11 mol/L. As for illite, the recovery of RE ions is lower than on halloysite when $(\text{NH}_4)_2\text{SO}_4$ concentration is 0.011 mol/L, implying that desorption of RE ions from illite is harder for kinetics. Based on these results, the optimal $(\text{NH}_4)_2\text{SO}_4$ concentration for halloysite and illite is 0.11 mol/L.

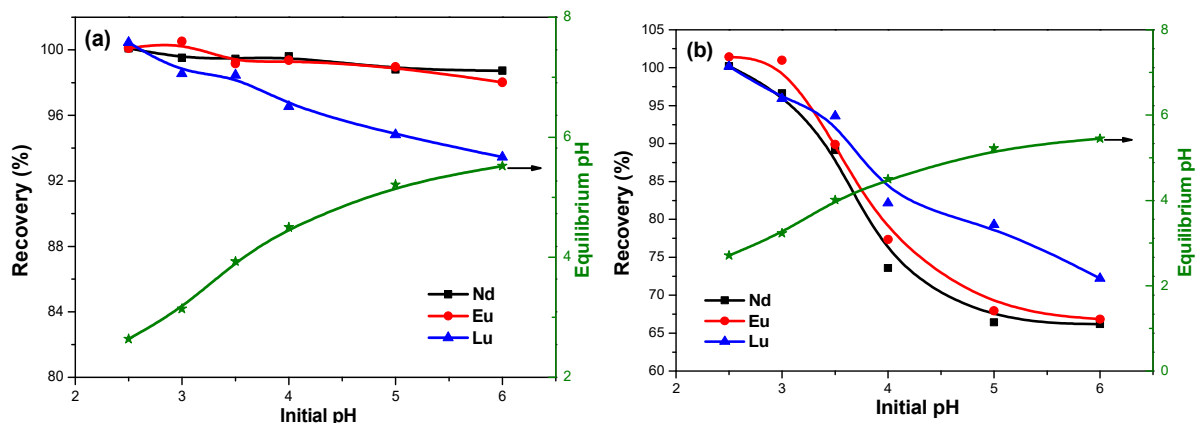


Figure 10. Influence of pH on the recovery of Nd^{3+} , Eu^{3+} and Lu^{3+} from halloysite (a) and illite (b). (Contact time = 240 min, $(\text{NH}_4)_2\text{SO}_4$ concentration = 0.11 mol/L.)

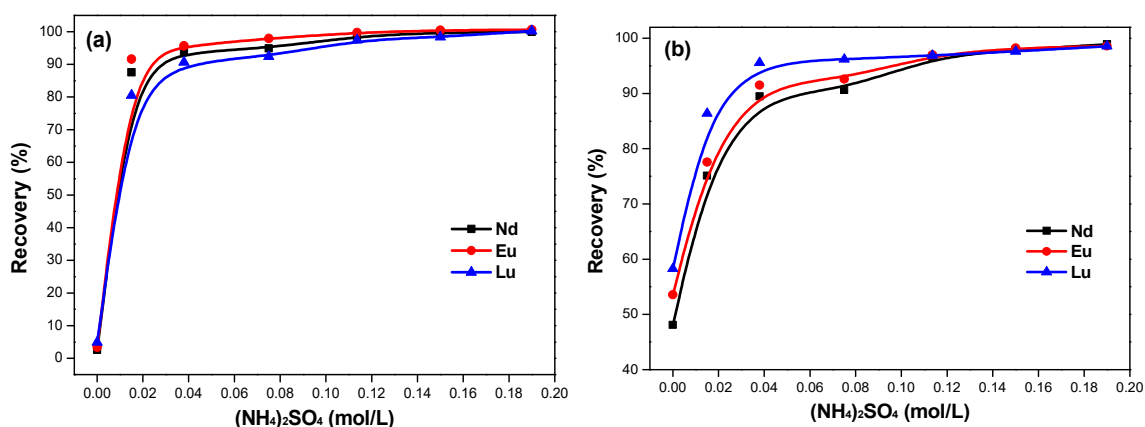


Figure 11. Influence of $(\text{NH}_4)_2\text{SO}_4$ concentration on the recovery of Nd^{3+} , Eu^{3+} and Lu^{3+} from halloysite (a) and illite (b). (Contact time = 240 min, pH levels for halloysite and illite are 4 and 3, respectively.)

3.3.4. Influence of Contact Time on RE Ion Desorption

The recovery of Nd^{3+} , Eu^{3+} and Lu^{3+} from halloysite and illite as a function of contact time is investigated, and the results are shown in Figure 12. The desorption efficiencies of RE ions from halloysite and illite are very fast, most of RE ions are desorbed within 5 min (~92%), and then slightly increase with an increase in contact time. A similar study reported that the leaching kinetics were very fast, within <5 min [35]. Process kinetics were found to be very fast; this fact can be attributed to an ion-exchange mechanism. The desorption rate of Lu^{3+} (heavy RE) is slower than Nd^{3+} (light RE), which may be due to the smaller ionic radius of Lu^{3+} .

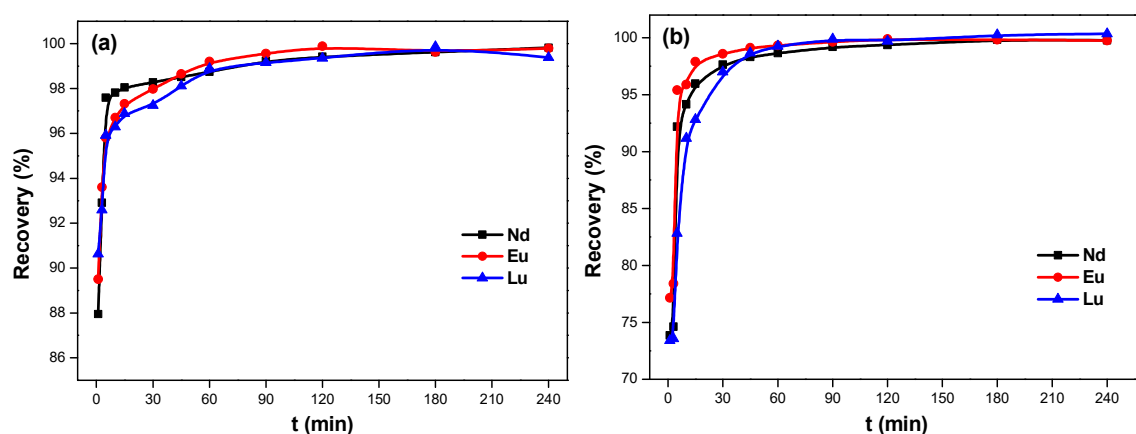


Figure 12. Influence of contact time on the recovery of Nd^{3+} , Eu^{3+} and Lu^{3+} from halloysite (a) and illite (b). (pH levels for halloysite and illite are 4 and 3, respectively, $(\text{NH}_4)_2\text{SO}_4$ concentration = 0.11 mol/L.)

3.4. Comparison

Based on the above results, there are obvious differences for the adsorption and desorption characteristics of RE ions from halloysite and illite, which are the primary clay minerals of ion-adsorption RE ore. Halloysite and illite are both silicate minerals, and surface hydroxyl can be protonated and deprotonated, which has a crucial effect on the adsorption mechanism of RE ions. The adsorption experiments reveal that RE ions were adsorbed on halloysite only through electrostatic attraction, while they were absorbed by electrostatic attraction and coordination bonds on illite. This may be due to the narrow interlamellar spacing of halloysite (7 Å), which prevents RE ions close to its surface from absorbing further. Hence, it is easy to desorb RE ions from halloysite, while more acidic solutions are needed for illite. The results could give some suggestions about the leaching technology of ion-adsorption RE ore: it seems possible to formulate distinctive leaching technologies depending on the clay mineral species of ion-adsorption RE ore. Since the species of clays change with an increase in depth, halloysite is usually distributed in the top (completely weathered layer), while illite appears in the bottom (partly weathered layer) [11]. If the clays of ion-adsorption RE ores are dominated by halloysite, the pH of a leaching agent can be lower than 4 and the leaching time can be very short, whereas the pH should be lower than 3 if there is a large amount of illite.

4. Conclusions

This study shows the adsorption/desorption characteristics of Nd^{3+} , Eu^{3+} and Lu^{3+} from halloysite and illite with various experimental conditions. The zeta potential of halloysite and illite is negative, which provided the driving force for adsorbing RE ions. The buffer pH is decreased after adsorbing RE ions. The kinetics adsorption and recovery were very fast, although the adsorption rate of halloysite is higher than illite; moreover, the adsorption process follows the pseudo-second-order kinetic model. The adsorption capacity of halloysite and illite increases with the increase of adsorption pH and remains a constant when pH higher than 4. The adsorption pH has a significant effect on the adsorption stability of RE ions onto illite, while it makes no difference for halloysite. On account of the narrow interlamellar spacing and nanotube nature of halloysite, RE ions were adsorbed on halloysite only by electrostatic attraction, whereas electrostatic attraction and coordination bonds are formed between RE ions and illite, due to the deprotonation of illite surfaces. The recovery of Nd^{3+} , Eu^{3+} and Lu^{3+} from halloysite decreased slightly with an increase in desorption pH, while it decreased more drastically for illite. The desorption efficiencies of RE ions from halloysite and illite are very fast (within 5 min).

The results of this work are of benefit for better understanding the mechanisms that influence the adsorption/desorption characteristics of the RE ions onto halloysite and illite. This study also provided a potential project: leaching RE ions from ion-adsorption RE ore depending on the species of clay minerals, which can reduce the use of leaching agents to become more eco-friendly. It seems feasible to build dumps that are composed by ion-adsorption RE ores which are unearthed in the same depth, and then use leaching technologies depending on clay species.

Author Contributions: S.Q.: Data curation, Formal analysis, Funding acquisition, Writing—original draft; H.Y.: Project administration, Writing—review & editing; B.H.: Resources; Q.L.: Investigation; J.X.: Software; F.L.: Resources; L.T.: Resources; X.Z.: Visualization; T.Q.: Funding acquisition. All authors have read and agreed to the published version of the manuscript.

Funding: National Natural Science Foundation of China (No. 52004107), Collaborative Innovation Center for Development and Utilization of Rare Metal Resources Co-sponsored by Ministry of Education and Jiangxi Province, Jiangxi University of Science and Technology, China (JXUST-XTX-2022-01), and the Key research and development program of Jiangxi Province, China (20212BBG73049).

Conflicts of Interest: The authors declare no conflict of interest.

References

1. Brown, B.; Ma, B.M.; Chen, Z.M. Developments in the processing and properties of NdFeB-type permanent magnets. *J. Magn. Magn. Mater.* **2002**, *248*, 432–440. [\[CrossRef\]](#)
2. Qiao, J.; Zhao, J.; Liu, Q.; Xia, Z. Recent advances in solid-state LED phosphors with thermally stable luminescence. *J. Rare Earth* **2019**, *37*, 565–572. [\[CrossRef\]](#)
3. Zhang, N.Q.; Yan, H.; Li, L.; Wu, R.; He, H. Use of rare earth elements in single-atom site catalysis: A critical review—Commemorating the 100th anniversary of the birth of Academician Guangxian Xu. *J. Rare Earth* **2021**, *39*, 233–242. [\[CrossRef\]](#)
4. Bohlen, J.; Nürnberg, M.; Senn, J.W.; Letzig, D.; Agnew, S.R. The texture and anisotropy of magnesium–zinc–rare earth alloy sheets. *Acta Mater.* **2007**, *55*, 2101–2112. [\[CrossRef\]](#)
5. Chi, R.A.; Tian, J.; Li, Z.J.; Peng, C.; Wu, Y.X.; Li, S.R.; Wang, C.W.; Zhou, Z.A. Existing State and Partitioning of Rare Earth on Weathered Ores. *J. Rare Earth* **2005**, *23*, 756.
6. Braun, J.J.; Pagel, M.; Herbillin, A.; Rosin, C. Mobilization and redistribution of REEs and thorium in a syenitic lateritic profile: A mass balance study. *Geochim. Cosmochim. Acta* **1993**, *57*, 4419–4434. [\[CrossRef\]](#)
7. Price, R.C.; Gray, C.M.; Wilson, R.E.; Frey, F.A.; Taylor, S.R. The effects of weathering on rare earth element, Y and Ba abundances in Tertiary basalts from southeastern Australia. *Chem. Geol.* **1991**, *93*, 245–265. [\[CrossRef\]](#)
8. Nesbitt, H.W. Mobility and fractionation of rare earth elements during weathering of granodiorite. *Nature* **1979**, *279*, 206–210. [\[CrossRef\]](#)
9. Duddy, L.R. Redistribution and fractionation of rare earth and other elements in a weathering profile. *Chem. Geol.* **1980**, *30*, 363–381. [\[CrossRef\]](#)
10. Barnett, M.J.; Palumbo-Roe, B.; Gregory, S.P. Comparison of Heterotrophic Bioleaching and Ammonium Sulfate Ion Exchange Leaching of Rare Earth Elements from a Madagascan Ion-Adsorption Clay. *Minerals* **2018**, *8*, 236. [\[CrossRef\]](#)
11. Chi, R.A.; Tian, J. Review of Weathered Crust Rare Earth Ore. *J. Chin. Rare Earth Soc.* **2007**, *25*, 641–650.
12. Pebdani, M.H.; Miller, R.E. Molecular dynamics simulation of pull-out halloysite nanotube from polyurethane matrix. *Adv. Mech. Eng.* **2021**, *13*, 16878140211044663. [\[CrossRef\]](#)
13. Jin, J.; Assemi, S.; Asgar, H.; Gadikota, G.; Tran, T.; Nguyen, W.; McLennan, J.D.; Miller, J.D. Characterization of Natural Consolidated Halloysite Nanotube Structures. *Minerals* **2021**, *11*, 1308. [\[CrossRef\]](#)
14. Srodon, J. X-ray powder diffraction identification of illitic materials. *Clay Clay Min.* **1984**, *5*, 337–349. [\[CrossRef\]](#)
15. Tombácz, E. Adsorption from Electrolyte Solutions. In *Adsorption: Theory, Modeling, and Analysis*; Tóth, J., Ed.; Marcel Dekker: New York, NY, USA, 2002; pp. 711–742.
16. Gładysz-Płaska, A.; Majdan, M.; Grabias, E. Adsorption of La, Eu and Lu on raw and modified red clay. *J. Radioanal. Nucl. Chem.* **2014**, *301*, 33–40. [\[CrossRef\]](#)
17. Iannicelli-Zubiani, E.M.; Cristiani, C.; Dotelli, G.; Gallo Stampino, P.; Pelosato, R.; Mesto, E.; Schingaro, E.; Lacalamita, M. Use of natural clays as sorbent materials for rare earth ions: Materials characterization and set up of the operative parameters. *Waste Manag.* **2015**, *46*, 546–556. [\[CrossRef\]](#)
18. Anastopoulos, I.; Bhatnagar, A.; Lima, E.C. Adsorption of rare earth metals: A review of recent literature. *J. Mol. Liq.* **2016**, *221*, 954–962. [\[CrossRef\]](#)
19. Gao, Y.H.; Fan, Z.C.; Xu, H.; Wang, L. An experimental study of the characteristics of REE adsorption of kaolinite and halloysite-7A. *Acta Petrol. Et Miner.* **2018**, *37*, 161–168.

20. Yang, M.; Liang, X.; Ma, L.; Huang, J.; He, H.; Zhu, J. Adsorption of REEs on kaolinite and halloysite: A link to the REE distribution on clays in the weathering crust of granite. *Chem. Geol.* **2019**, *525*, 210–217. [\[CrossRef\]](#)
21. Alshameri, A.; He, H.; Xin, C.; Zhu, J.; Xinghu, W.; Zhu, R.; Wang, H. Understanding the role of natural clay minerals as effective adsorbents and alternative source of rare earth elements: Adsorption operative parameters. *Hydrometallurgy* **2019**, *185*, 149–161. [\[CrossRef\]](#)
22. Wang, Q.; Ma, L.; Huang, K.J.; Lei, Z.Y.; Xie, S.Y. Quantitative Analysis of Kaolinite, Illite and Montmorillonite by X-ray Diffraction. *Guizhou Geol.* **2021**, *38*, 71–78.
23. Chen, Y.; Zhu, C.; Sun, Y.; Duan, H.; Ye, W.; Wu, D. Adsorption of La(III) onto GMZ bentonite: Effect of contact time, bentonite content, pH value and ionic strength. *J. Radioanal. Nucl. Chem.* **2012**, *292*, 1339–1347. [\[CrossRef\]](#)
24. Wu, D.B.; Zhu, C.; Chen, Y.; Zhu, B.; Yang, Y.; Wang, Q.; Ye, W. Preparation, characterization and adsorptive study of rare earth ions using magnetic GMZ bentonite. *Appl. Clay Sci.* **2012**, *62*, 87–93. [\[CrossRef\]](#)
25. Alshameri, A.; He, H.; Zhu, J.; Xi, Y.; Zhu, R.; Ma, L.; Tao, Q. Adsorption of ammonium by different natural clay minerals: Characterization, kinetics and adsorption isotherms. *Appl. Clay Sci.* **2018**, *159*, 83–93. [\[CrossRef\]](#)
26. Alshameri, A.; Ibrahim, A.; Assabri, A.M.; Lei, X.; Wang, H.; Yan, C. The investigation into the ammonium removal performance of Yemeni natural zeolite: Modification, ion exchange mechanism, and thermodynamics. *Powder Technol.* **2014**, *258*, 20–31. [\[CrossRef\]](#)
27. Lagergren, S. Zur theorie der sogenannten adsorption gelöster stoffe. *K. Sven. Vetenskapsakad. Handl.* **1898**, *24*, 1–39.
28. Ho, Y.S.; McKay, G.J.P.B. Pseudo-second order model for sorption processes. *J Process Biochem.* **1999**, *34*, 451–465. [\[CrossRef\]](#)
29. Zhou, F.; Huang, S.H.; Liu, X.; Feng, J.; Liu, Q.; Wang, Z.W.; Li, C.C.; Xu, Y.L. Adsorption kinetics and thermodynamics of rare earth on Montmorillonite modified by sulfuric acid. *Colloid. Surf. A Physicochem. Eng. Asp.* **2021**, *627*, 127063.
30. Wang, Y.Q.; Zhang, Z.B.; Li, Q.; Liu, Y.H. Adsorption of uranium from aqueous solution using HDTMA+-pillared bentonite: Isotherm, kinetic and thermodynamic aspects. *J. Radioanal. Nucl. Chem.* **2012**, *293*, 231–239. [\[CrossRef\]](#)
31. Peng, C.; Zhong, Y.; Wang, G.; Min, F.; Qin, L. Atomic-level insights into the adsorption of rare earth $Y(OH)_{3-n}^{n+}$ ($n = 1-3$) ions on kaolinite surface. *Appl. Surf. Sci.* **2019**, *469*, 357–367. [\[CrossRef\]](#)
32. Wang, G.S.; Lai, Y.M.; Peng, C.L. Adsorption of rare earth yttrium and ammonium ions on kaolinite surfaces: A DFT study. *Theor. Chem. Acc.* **2018**, *137*, 53. [\[CrossRef\]](#)
33. Qiu, S.; Qiu, T.S.; Yan, H.S.; Long, Q.B.; Wu, H.; Li, X.B.; Zhu, D.M. Investigation of protonation and deprotonation processes of kaolinite and its effect on the adsorption stability of rare earth elements. *Colloid. Surf. A.* **2022**, *642*, 128596. [\[CrossRef\]](#)
34. Qiu, S.; Wu, H.; Yan, H.S.; Li, X.B.; Zhou, X.W.; Qiu, T.S. Theoretical investigation of hydrated $[Lu(OH)_2]^+$ adsorption on kaolinite(0 0 1) surface with DFT calculations. *Appl. Surf. Sci.* **2021**, *565*, 150473. [\[CrossRef\]](#)
35. Moldoveanu, G.A.; Papangelakis, V.G. Recovery of rare earth elements adsorbed on clay minerals: II. Leaching with ammonium sulfate. *Hydrometallurgy* **2013**, *131*, 158–166. [\[CrossRef\]](#)